Gate Tuning of Electronic Phase Transitions in Two-Dimensional $NbSe_2$

Xiaoxiang Xi,[1] Helmuth Berger,[2] László Forró,[2] Jie Shan,[1,*] and Kin Fai Mak[1,†]
[1]Department of Physics and Center for 2-Dimensional and Layered Materials, The Pennsylvania State University, University Park, Pennsylvania 16802-6300, USA
[2]Institute of Condensed Matter Physics, Ecole Polytechnique Fédérale de Lausanne, 1015 Lausanne, Switzerland

(Received 12 April 2016; published 29 August 2016)

Recent experimental advances in atomically thin transition metal dichalcogenide (TMD) metals have unveiled a range of interesting phenomena including the coexistence of charge-density-wave (CDW) order and superconductivity down to the monolayer limit. The atomic thickness of two-dimensional (2D) TMD metals also opens up the possibility for control of these electronic phase transitions by electrostatic gating. Here, we demonstrate reversible tuning of superconductivity and CDW order in model 2D TMD metal $NbSe_2$ by an ionic liquid gate. A variation up to ~50% in the superconducting transition temperature has been observed. Both superconductivity and CDW order can be strengthened (weakened) by increasing (reducing) the carrier density in 2D $NbSe_2$. The doping dependence of these phase transitions can be understood as driven by a varying electron-phonon coupling strength induced by the gate-modulated carrier density and the electronic density of states near the Fermi surface.

DOI: 10.1103/PhysRevLett.117.106801

In metals, the interactions between free carriers and ions that form the crystal structure lead to a multitude of many-body electronic phases [1]. Modifying the free carrier density, and thus the density of states (DOS) near the Fermi surface and screening of the interactions, has long been sought to control the electronic phases [2]. Electrostatic gating is a clean and reversible method to introduce doping near the surface of a material [3]. In particular, electric-double-layer based on an ionic liquid has had a tremendous success in doping various insulator surfaces into metallic phases [4–15]. However, little success has been made on significantly changing the carrier density in metals by electrostatic gating due to screening arisen from the extremely high carrier densities [16–18]. Recent experimental advances in atomically thin transition metal dichalcogenide (TMD) metals have unveiled a range of interesting collective electronic phenomena, including the coexistence of charge-density-wave (CDW) order and superconductivity down to the monolayer limit [19–21], a Bose metal phase [22], and Ising pairing in superconductivity [23]. The atomic thickness of two-dimensional (2D) TMD metals has also provided an ideal system to explore electrostatic doping and control of the collective electronic phases in the high-density metallic regime, where the high electronic DOS leads to multiple electronic instabilities.

2H-$NbSe_2$ is a representative TMD metal made of layers bonded by van der Waals' interactions [24]. Each single $NbSe_2$ layer (half of a unit cell thickness) consists of a layer of transition metal Nb atoms sandwiched between two layers of chalcogen Se atoms, forming a trigonal prismatic structure. The electronic band structure near the Fermi surface shows multiple pockets formed by the valence Bloch states [Fig. 1(a) for bilayer $NbSe_2$] [25]. 2H-$NbSe_2$ is a hole metal at room temperature. It undergoes a CDW and superconducting transition, respectively, at ~33 and 7 K in the bulk, with the two collective phases coexisting below 7 K [24]. Because of the weak interlayer van der Waals' bonding, $NbSe_2$ has been successfully exfoliated into atomically thin layers [19,20,22,23,26,27]. Monolayer $NbSe_2$ has also been grown on graphene by molecular beam epitaxy (MBE) [21]. With decreasing layer thickness, whereas all studies consistently show a decreasing superconducting transition temperature T_{C0}, detailed values vary among samples of different origin [19–23]. A large discrepancy also exists in the reported CDW transition temperature T_{CDW}. For instance, Xi *et al.* observed strongly enhanced CDW order in atomically thin $NbSe_2$ with $T_{CDW} > 100$ K for exfoliated monolayer samples [19]. Ugeda *et al.* reported slightly weakened CDW order ($T_{CDW} \sim 25$ K) in monolayer $NbSe_2$ grown on graphene [21]. These discrepancies are not well understood although sample quality and substrates are believed to play a role.

In this Letter, we employ transport and magnetotransport measurements to investigate the superconducting and CDW phase transition in 2D $NbSe_2$ as a function of carrier density modulated by ionic liquid gating. We have been able to *reversibly* tune the carrier density in bilayer $NbSe_2$ by up to 6×10^{14} cm^{-2} (~30% of the intrinsic density), and the superconducting transition temperature by ~50%, with enhanced (weakened) T_{C0} for hole (electron) doping. Although the precise value of T_{CDW} cannot be determined, a similar trend with doping has been observed. The observed doping dependence of the superconducting and CDW transition can be understood as a result of electron-phonon (e-ph) coupling modulated by the carrier density and the corresponding electronic DOS near the Fermi surface. Our results show that unintentional doping could contribute to the discrepancies among the reported critical temperatures.

 © 2016 American Physical Society

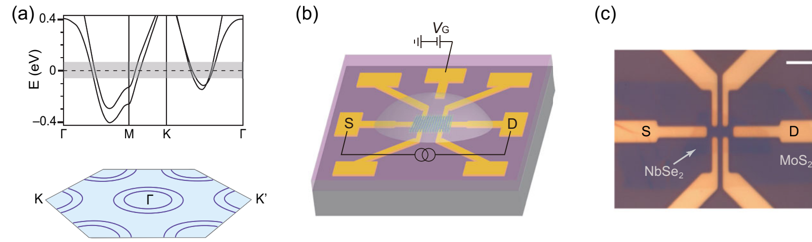

FIG. 1. (a) Top: Electronic band structure of undoped bilayer $NbSe_2$ reproduced from *ab initio* calculations of Ref. [25]. The dashed line indicates the Fermi level at zero gate voltage and the shaded region represents the range of Fermi levels accessible by gating in our experiment. Bottom: Schematic of the first Brillouin zone and the Fermi surface around the, Γ, K, and K' point. (b) Device schematic: Current was excited through electrode S and D; longitudinal and transverse voltage drops were measured; gate voltage V_G was supplied through an isolated electrode from the sample. (c) Optical image of a bilayer $NbSe_2$/monolayer MoS_2 stack on a Si substrate with gold electrodes before drop casting the ionic liquid. Scale bar is 5 μm.

In contrast to previous studies on gate-induced superconductivity in electron-doped MoS_2 [8,10,11,15], our work focuses on a high-density hole-doped regime, in which the Fermi level is located near the middle of the valence bands [Fig. 1(a)] with a much higher electronic DOS and stronger spin-orbit interactions. We also note that while pressure tuning of the CDW and superconducting transitions in bulk $NbSe_2$ has been demonstrated [28–30], our study examines continuous electrical tuning of these transitions in 2D $NbSe_2$ over a large window of doping densities, which is not accessible in bulk metallic materials.

Atomically thin $NbSe_2$ is known to be unstable under ambient conditions [19,20,22,23,27]. In fact, recent advances on the study of its intrinsic properties have been made possible only by capping $NbSe_2$ [19,20,22,23] or performing *in situ* measurements [21]. In recent gating studies of relatively thick $NbSe_2$ flakes using an ionic liquid [31,32], $NbSe_2$ flakes were brought into direct contact with the ionic liquid and an irreversible behavior was observed at high gate voltages. This is presumably caused by electrochemistry on the surfaces of $NbSe_2$. To protect the 2D $NbSe_2$ samples from oxidation and undesired electrochemistry in ionic liquid gating while maintaining the high gate capacitance of the device, we have introduced an ultrathin capping layer of a chemically stable large-gap semiconductor [33,34] or insulator [13,14]. Both MoS_2 monolayers and ultrathin (~1 nm) hexagonal boron nitride (hBN) layers have been tested. Within the gate voltage range of interest, they have produced similar results (Supplemental Material, Sec. I [35]). We have mainly used monolayer MoS_2 since it is much easier to identify than ultrathin hBN based on optical reflectance in the visible.

The fabrication method of 2D $NbSe_2$ devices has been described elsewhere [23]. In brief, atomically thin $NbSe_2$ samples were mechanically exfoliated from bulk single crystals on silicone elastomer polydimethylsiloxane (PDMS) substrates. Their thickness was first identified by the optical reflectance contrast and later confirmed by Raman spectroscopy [19]. The samples were then transferred onto silicon substrates with pre-patterned Au electrodes and shaped into a Hall bar geometry by removing unwanted areas using a polypropylene carbonate (PPC) layer on a PDMS stamp. Capping layers prepared on separate substrates were subsequently transferred onto $NbSe_2$. Ionic liquid *N*,*N*-diethyl-*N*-(2-methoxyethyl)-*N*-methylammonium bis(trifluoromethylsulphonyl-imide) (DEME-TFSI) was finally drop casted, covering both the sample and the gate electrode. The schematic and optical microscope image of a typical device are shown in Figs. 1(b) and 1(c), respectively. The finished devices were annealed at 350 K in high vacuum for 3–5 h to dehydrate the ionic liquid and to ensure good interfacial contacts between different layers. Since it is much easier to fabricate high-quality bilayer than monolayer devices, we focus our study on $NbSe_2$ bilayers. Similar results but stronger effects are expected for monolayers.

Transport measurements were carried out in a Physical Property Measurement System down to 2.1 K. Both longitudinal sheet resistance (R_s) and transverse sheet resistance (R_t) were acquired with excitation currents limited to 1 μA to avoid the heating and high-bias effects. Because of the finite longitudinal-transverse coupling in our devices and the presence of magnetoresistance at low temperature, we antisymmetrized the transverse sheet resistance under magnetic field H of opposite directions to obtain the Hall resistance, $R_{xy}(H) = [(R_t(H) - R_t(-H))/2]$, and the sheet Hall coefficient, $R_H = (R_{xy}/H)$. (See Supplemental Material, Sec. II for more details [35].) To vary the doping density, gate voltage was adjusted at 220 K (which is near the freezing point of the ionic liquid [8]), followed by rapid cooling to minimize any electrochemistry effects.

Figure 2 shows the temperature dependence of the sheet resistance R_s under zero magnetic field and the sheet Hall coefficient R_H of a typical device (No. 120) under gate voltage V_G varying from −2 to 3 V. Metallic behavior is seen in the temperature dependence of R_s [Fig. 2(a)]: R_s scales linearly with temperature T due to e-ph scattering at high temperature, and saturates to a residual value of about 250 Ω due to impurity or defect scattering at low temperature. The residual-resistance ratio (RRR) [estimated as $(R_s(300\ \mathrm{K})/R_s(8\ \mathrm{K}))$] is about 6. Further cooling causes a rapid drop of R_s to zero below 5 K, indicating a superconducting transition. Figure 2(b) clearly shows that T_{C0} shifts by ~30% under gate voltage varying from −2 to 3 V. This modification

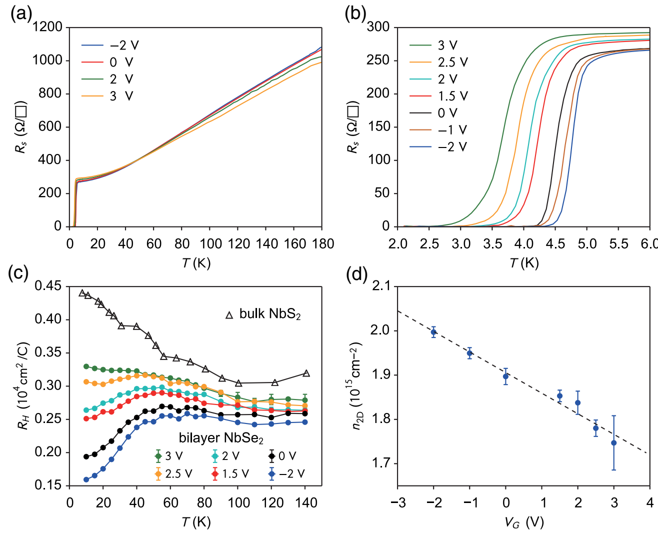

FIG. 2. (a)–(c) Temperature dependence of the longitudinal sheet resistance (a), (b) and the sheet Hall coefficient (c) at selected gate voltages. Longitudinal sheet resistance across the superconducting transition is shown in (b). Data from bulk NbS_2 [38] are also shown as empty triangles in (c). (d) Gate voltage dependence of the sheet carrier density. The error bars are estimated from the uncertainties in the sheet Hall coefficient. The dashed line is a linear fit. All data are from device No. 120.

is in contrast to previous experiments based on silicon or oxide back gates, where very small modulations in T_{C0} (<0.2 K) have been reported [20,27,42]. Similarly, R_H also depends strongly on gate voltage [Fig. 2(c)]: for $T > 100$ K, R_H is largely temperature independent; its value increases with increasing V_G. For $T < 100$ K, a drop in R_H upon cooling is observed under V_G up to ~2 V; the drop in R_H eventually turns into a rise under large positive V_G's. As we discuss below, the high-temperature behavior of R_H is dominated by the carrier density and will be used to evaluate its value; and the low-temperature behavior is influenced by the CDW transition.

Before we interpret the above results, we preform multiple control experiments. (See Supplemental Material, Sec. I for details [35].) First, we test the reversibility of the effect. Six bilayer devices have been tested under different gating sequences. All of them were highly reversible and repeatable under the gate voltage range of −2 to 3 V. (Some devices withstood higher gate voltages, e.g., No. 150.) Thus, extrinsic effects such as gate-induced electrochemistry are unlikely the origin of the observed effects. Second, we compare ionic liquid gating with conventional solid-state dielectric gating by fabricating a bilayer $NbSe_2$ device with a combination of a Si/SiO_2 back gate and a graphene/hBN top gate. Similar effects on T_{C0}, but much smaller modulations, have been observed. Third, we verify the role of the MoS_2 capping layer. To exclude the possibility of gate-induced superconductivity in MoS_2, as has been recently demonstrated [8,10,11,15], we have performed an identical experiment on monolayer MoS_2 alone. No gate-induced superconductivity was observed within the gate voltage range employed in this work. The MoS_2 film thus only serves as a protection layer similar to ultrathin hBN. Finally, we note that in addition to doping, electrostatic gating with a single gate also introduces a vertical electric field on the samples. The device with dual solid-state gates showed that the electric-field effect on the electronic phase transitions is negligible compared to the doping effect. We therefore only consider the doping effects in $NbSe_2$ below.

We now extract the doping dependence of the superconducting transition temperature of bilayer $NbSe_2$. For simplicity, we have taken T_{C0} to be the temperature corresponding to half of the normal state resistance (see Supplemental Material, Sec. III for more accurate determinations of T_{C0} and for current excitation measurements at varying temperatures [35]). To extract the total sheet density n_{2D}, we have used the high-temperature (>100 K) value of the Hall coefficient R_H. Although $NbSe_2$ is a multiband metal, it has been shown that at high temperature the carrier scattering rate becomes isotropic in the Fermi surface and R_H can provide a good estimate of the carrier density by using $n_{2D} = (f/eR_H)$ [43]. Here, e is the elementary charge, and f is a dimensionless parameter close to unity. A value of $f \approx 0.8$ has been obtained by calibrating n_{2D} at $V_G = 0$ V to the known carrier density n_0 in bulk $NbSe_2$: $n_{2D} = n_0 t \approx 1.9 \times 10^{15}$ cm^{-2} ($n_0 \approx 1.5 \times 10^{22}$ cm^{-3} corresponds to 1 hole per Nb atom and $t \approx 1.25$ nm is the bilayer thickness [24]). We note that in the above calibration we have ignored charge transfer between MoS_2 and $NbSe_2$ due to their work function mismatch, which has been estimated $<10^{13}$ cm^{-2}. The V_G dependence of n_{2D} is shown in Fig. 2(d) (symbols), which follows a linear dependence (dashed line). The negative slope is consistent with the fact that $NbSe_2$ is a hole metal. We calculate the gate capacitance from the slope to be 7 μF/cm^2. The value agrees very well with the reported ones for the same ionic liquid [8]. The corresponding tuning range of the Fermi energy, calibrated from the DOS at the Fermi surface from *ab initio* calculations [25], is ~130 meV [shaded region in the electronic band structure of Fig. 1(a)].

Figure 3(a) summarizes the doping dependence of T_{C0} for three bilayer devices. It clearly shows a monotonic dependence of T_{C0} on (hole) density and the ability of gate tuning of T_{C0} from 2.8 to 5.2 K (4.5 K for undoped case), which correspond to a modulation of ~50%. In Fig. 3(b) we show the perpendicular critical field ($H_{C2\perp}$)—critical temperature (T_C) phase diagram at different doping levels. Following the same convention used for zero magnetic field, we have determined T_C at half of the normal state resistance. We note that the $H_{C2\perp} - T_C$ phase diagram is complicated by the enhanced vortex fluctuation effects in two dimensions, giving rise to much broadened superconducting transitions under finite magnetic fields (see Supplemental Material, Sec. IV [35]) [22,36]. Near T_{C0}, the $H_{C2\perp} - T_C$ dependences are well described by a linear relation $H_{C2\perp} = (\Phi_0/2\pi\xi_0^2)(1-(T_C/T_{C0}))$ (solid lines), where Φ_0 and ξ_0 denote the flux quantum and the superconducting coherence length, respectively [22,36]. The

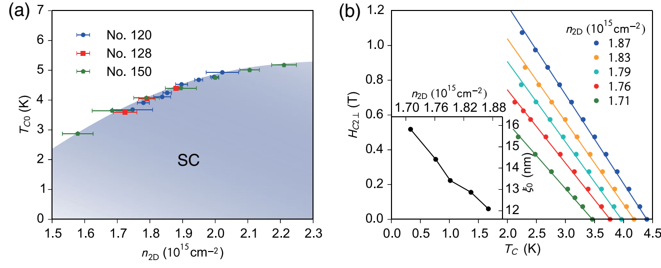

FIG. 3. (a) T_{C0}-n_{2D} phase diagram of bilayer $NbSe_2$. The horizontal error bars originate from the measurement uncertainty of the Hall coefficient. The filled area corresponding to the superconducting (SC) phase is a guide to the eye. (b) $H_{C2\perp}$-T_C phase diagram of bilayer $NbSe_2$ under a magnetic field perpendicular to the sample at different doping levels. The symbols are T_C determined as the temperature corresponding to 50% of the normal state resistance. The lines are linear fits. The inset shows the carrier density dependence of the zero-temperature coherence length extracted from the linear fits.

magnitude of the slope increases with increasing T_{C0}, from which the superconducting coherent length ξ_0 can be determined to decrease with T_{C0}, equivalently, also with the hole density [inset, Fig. 3(b)]. Furthermore, the increasing slope also projects a higher upper critical field (at $T = 0$) with increasing T_{C0} [36]. This finding in bilayer $NbSe_2$ is distinct from that in bulk $NbSe_2$ under high pressure, where the upper critical field has been observed to decrease with increasing T_{C0} [29]. We note that unlike the anomalous behavior under high pressure that requires a complete two-band model to understand, superconductivity in bulk $NbSe_2$ under low pressure can be described by a simple one-band approximation since e-ph coupling in one of the bands dominates [29]. Below we compare our experiment to the simple one-band model.

Superconductivity in bulk $NbSe_2$ is known to be the BCS type driven by e-ph interactions. In the one-band model, T_{C0} is predicted by the strong-coupling formula as [44]

$$T_{C0} = \frac{\omega_{\log}}{1.2}\exp\left[-\frac{1.04(1+\lambda)}{\lambda - \mu^*(1+0.62\lambda)}\right]. \tag{1}$$

Here, $\omega_{\log}$ is the weighted average of the phonon energies in Kelvin introduced by Allen and Dynes [44], μ^* is the Coulomb pseudopotential, and $\lambda = N(\epsilon_F)V_0$ is the dimensionless e-ph coupling constant with $N(\epsilon_F)$ and V_0 denoting, respectively, the electronic DOS at the Fermi energy ϵ_F and the effective e-ph coupling energy V_0. We evaluate the dimensionless e-ph coupling constant λ from the temperature dependence of the longitudinal resistance, specifically its slope dR_s/dT at high temperature [Fig. 2(a)]. Electron-phonon scattering in a 2D metal leads to $(dR_s/dT) = (2\pi\hbar n_0 k_B/\varepsilon_0 n_{2D}(\hbar\omega_{p0})^2)\lambda$, where, $\hbar$, k_B, ε_0, and $\hbar\omega_{p0}$ ($\approx$2.74 eV [37]) are the Planck's constant, Boltzmann constant, vacuum permittivity, and the in-plane plasma energy of bulk $NbSe_2$, respectively [1]. (See Supplemental Material, Sec. V for details [35]). The dependence of λ on carrier density n_{2D} is shown in Fig. 4(a). The dependence of T_{C0} on λ is shown in Fig. 4(b) (symbols). The latter can be reasonably well described by Eq. (1) with $\omega_{\log} \approx 50$ K and $\mu^* \approx 0.10$ (solid line). The value of $\omega_{\log}$ agrees well with the reported one from the layer thickness dependence of T_{C0} for 2D $NbSe_2$ [23]. The value of μ^* is consistent with the estimate $\mu^* \approx (0.26N(\epsilon_F)/1 + N(\epsilon_F)) \approx 0.15$ [45] from the DOS at the Fermi energy from *ab initio* calculations for undoped $NbSe_2$ [25].

Finally, we comment on the CDW order in 2D $NbSe_2$. A kink in the longitudinal resistance R_S and a drop (even a change of sign for high-quality samples) in the Hall coefficient R_H around T_{CDW} upon cooling due to Fermi surface instability [46,47] have been established and widely used as the transport signature of the CDW transition in bulk isoelectronic group-V TMDs (2H-$NbSe_2$, $TaSe_2$, NbS_2, and TaS_2) [30,38]. Among these compounds, NbS_2 is known not to possess a CDW phase and its Hall coefficient shows a rise instead of a drop upon cooling [empty triangles, Fig. 2(c)] [24,38], and $TaSe_2$ is known to possess strong CDW signature in transport [30,38]. We have performed a doping dependence study of the CDW transition in both bilayer $NbSe_2$ (Fig. 2) and $TaSe_2$ (Supplemental Material, Sec. VI [35]). In the latter the strong CDW transition signature has allowed us to determine T_{CDW} and conclude that the CDW order is weakened with increasing V_G (decreasing hole density). In $NbSe_2$, the kink in R_S is significantly broadened and cannot be identified [Fig. 2(a)] presumably due to the sample's low RRRs. A drop in R_H is still observed for V_G up to ~2 V, but the amount of the drop decreases with V_G till reaching ~3 V, at which R_H increases monotonically upon cooling as observed in NbS_2 [Fig. 2(c)]. These observations provide strong evidence that the CDW order in bilayer $NbSe_2$ is also weakened with decreasing hole density and can potentially even be destroyed at large gate voltages.

The correlated dependence of superconductivity and CDW order on doping observed in our experiment suggests a peaceful coexistence of the 2 orders in 2D $NbSe_2$, in accord with the behavior in bulk $NbSe_2$ and related TMDs

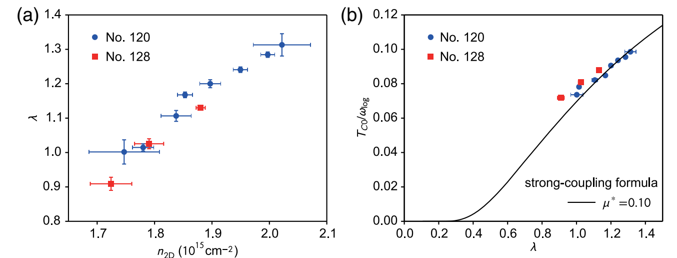

FIG. 4. (a) Dimensionless e-ph coupling constant as a function of sheet carrier density. The vertical and horizontal error bars are from fitting of the normal-state resistance to the e-ph scattering model and the measurement uncertainty of the Hall coefficient, respectively. (b) Superconducting transition temperature T_{C0} as a function of e-ph coupling constant λ for bilayer $NbSe_2$. The solid line is the best fit to the strong-coupling formula [Eq. (1)] with $\omega_{\log} = 50$ K and $\mu^* = 0.10$.

revealed by recent high-pressure studies [29,30]. Angle-resolved photoemission spectroscopy [48] shows that while anisotropic s-wave superconducting gaps are opened at the $NbSe_2$ Fermi surface, CDW gaps are opened only near the CDW wave vectors, where the superconducting gap is minimum; the 2 orders thus have minimum effects on each other. The influence of the anisotropic CDW gap on the superconducting gap has also been investigated by scanning tunneling microscopy experiments [49]. Future studies on 2D $NbSe_2$ or similar systems by introducing higher hole doping densities so that the Fermi level approaches the saddle point singularity at the M point of the Brillouin zone [25] would be very interesting. It may lead to drastic changes and even new phenomena in the collective electronic phases such as a superconducting dome observed recently in heavily doped MoS_2 [8].

The experimental research was supported by the National Science Foundation through Grants No. DMR-1645901 (sample and device fabrication), DMR-1410407 (optical characterization), and the Air Force Office of Scientific Research under Grant No. FA9550-16-1-0249 (transport measurements). Support for data analysis was provided by the U.S. Department of Energy, Office of Basic Energy Sciences Contracts No. DESC0012635 (J. S.) and No. DESC0013883 (K. F. M.). The work in Lausanne was supported by the Swiss National Science Foundation.

*Corresponding author.
jus59@psu.edu
†Corresponding author.
kzm11@psu.edu

[1] G. Grimvall, *The Electron-Phonon Interaction in Metals* (North-Holland Publishing Co., Amsterdam, 1981).
[2] R. E. Glover, III and M. D. Sherrill, Phys. Rev. Lett. **5**, 248 (1960).
[3] C. H. Ahn *et al.*, Rev. Mod. Phys. **78**, 1185 (2006).
[4] K. Ueno, S. Nakamura, H. Shimotani, A. Ohtomo, N. Kimura, T. Nojima, H. Aoki, Y. Iwasa, and M. Kawasaki, Nat. Mater. **7**, 855 (2008).
[5] A. T. Bollinger, G. Dubuis, J. Yoon, D. Pavuna, J. Misewich, and I. Bozovic, Nature (London) **472**, 458 (2011).
[6] Y. Lee, C. Clement, J. Hellerstedt, J. Kinney, L. Kinnischtzke, X. Leng, S. D. Snyder, and A. M. Goldman, Phys. Rev. Lett. **106**, 136809 (2011).
[7] X. Leng, J. Garcia-Barriocanal, S. Bose, Y. Lee, and A. M. Goldman, Phys. Rev. Lett. **107**, 027001 (2011).
[8] J. T. Ye, Y. J. Zhang, R. Akashi, M. S. Bahramy, R. Arita, and Y. Iwasa, Science **338**, 1193 (2012).
[9] M. Yoshida, Y. Zhang, J. Ye, R. Suzuki, Y. Imai, S. Kimura, A. Fujiwara, and Y. Iwasa, Sci. Rep. **4**, 7302 (2014).
[10] Y. Saito *et al.*, Nat. Phys. **12**, 144 (2016).
[11] J. M. Lu, O. Zheliuk, I. Leermakers, N. F. Q. Yuan, U. Zeitler, K. T. Law, and J. T. Ye, Science **350**, 1353 (2015).
[12] Y. J. Yu *et al.*, Nat. Nanotechnol. **10**, 270 (2015).
[13] L. J. Li, E. C. T. O'Farrell, K. P. Loh, G. Eda, B. Özyilmaz, and A. H. Castro Neto, Nature (London) **529**, 185 (2016).
[14] P. Gallagher, M. Lee, T. A. Petach, S. W. Stanwyck, J. R. Williams, K. Watanabe, T. Taniguchi, and D. Goldhaber-Gordon, Nat. Commun. **6**, 6437 (2015).
[15] D. Costanzo, S. Jo, H. Berger, and A. F. Morpurgo, Nat. Nanotechnol. **11**, 339 (2016).
[16] J. Choi, R. Pradheesh, H. Kim, H. Im, Y. Chong, and D.-H. Chae, Appl. Phys. Lett. **105**, 012601 (2014).
[17] M. Sagmeister, U. Brossmann, S. Landgraf, and R. Würschum, Phys. Rev. Lett. **96**, 156601 (2006).
[18] T. A. Petach, M. Lee, R. C. Davis, A. Mehta, and D. Goldhaber-Gordon, Phys. Rev. B **90**, 081108 (2014).
[19] X. Xi, L. Zhao, Z. Wang, H. Berger, L. Forró, J. Shan, and K. F. Mak, Nat. Nanotechnol. **10**, 765 (2015).
[20] Y. Cao *et al.*, Nano Lett. **15**, 4914 (2015).
[21] M. M. Ugeda *et al.* Nat. Phys. **12**, 92 (2016).
[22] A. W. Tsen, B. Hunt, Y. D. Kim, Z. J. Yuan, S. Jia, R. J. Cava, J. Hone, P. Kim, C. R. Dean, and A. N. Pasupathy, Nat. Phys. **12**, 208 (2016).
[23] X. Xi, Z. Wang, W. Zhao, J.-H. Park, K. T. Law, H. Berger, L. Forró, J. Shan, and K. F. Mak, Nat. Phys. **12**, 139 (2016).
[24] J. A. Wilson, F. J. Di Salvo, and S. Mahajan, Adv. Phys. **50**, 1171 (2001).
[25] M. Calandra, I. I. Mazin, and F. Mauri, Phys. Rev. B **80**, 241108 (2009).
[26] R. F. Frindt, Phys. Rev. Lett. **28**, 299 (1972).
[27] N. E. Staley, J. Wu, P. Eklund, Y. Liu, L. J. Li, and Z. Xu, Phys. Rev. B **80**, 184505 (2009).
[28] C. W. Chu, V. Diatschenko, C. Y. Huang, and F. J. DiSalvo, Phys. Rev. B **15**, 1340 (1977).
[29] H. Suderow, V. G. Tissen, J. P. Brison, J. L. Martínez, and S. Vieira, Phys. Rev. Lett. **95**, 117006 (2005).
[30] D. C. Freitas *et al.*, Phys. Rev. B **93**, 184512 (2016).
[31] Z. J. Li, B. F. Gao, J. L. Zhao, X. M. Xie, and M. H. Jiang, Supercond. Sci. Technol. **27**, 015004 (2014).
[32] M. Yoshida, J. Ye, T. Nishizaki, N. Kobayashi, and Y. Iwasa, Appl. Phys. Lett. **108**, 202602 (2016).
[33] K. F. Mak, C. Lee, J. Hone, J. Shan, and T. F. Heinz, Phys. Rev. Lett. **105**, 136805 (2010).
[34] A. Splendiani, L. Sun, Y. Zhang, T. Li, J. Kim, C.-Y. Chim, G. Galli, and F. Wang, Nano Lett. **10**, 1271 (2010).
[35] See Supplemental Material http://link.aps.org/supplemental/10.1103/PhysRevLett.117.106801 for details on control experiments, transport under a field, and analysis of the critical temperatures and the e-ph coupling, which includes Refs. [1,24,36–41].
[36] M. Tinkham, *Introduction to Superconductivity* (McGraw-Hill, New York, 1996), 2nd ed.
[37] S. V. Dordevic, D. N. Basov, R. C. Dynes, and E. Bucher, Phys. Rev. B **64**, 161103 (2001).
[38] M. Naito and S. Tanaka, J. Phys. Soc. Jpn. **51**, 219 (1982).
[39] T. Kumakura, H. Tan, T. Handa, M. Morishita, and H. Fukuyama, Czech. J. Phys. **46**, 2611 (1996).
[40] M. R. Beasley, J. E. Mooij, and T. P. Orlando, Phys. Rev. Lett. **42**, 1165 (1979).
[41] L. G. Aslamasov and A. I. Larkin, Phys. Lett. A **26**, 238 (1968).
[42] M. S. El-Bana, D. Wolverson, S. Russo, G. Balakrishnan, D. M. Paul, and S. J. Bending, Supercond. Sci. Technol. **26**, 125020 (2013).
[43] N. P. Ong, Phys. Rev. B **43**, 193 (1991).

[44] P. B. Allen and R. C. Dynes, Phys. Rev. B **12**, 905 (1975).
[45] K. H. Benneman and J. W. Garland, *Superconductivity in d- and f-band Metals* (American Institute of Physics, College Park, MD, 1972), p. 103.
[46] R. Bel, K. Behnia, and H. Berger, Phys. Rev. Lett. **91**, 066602 (2003).
[47] L. Li, J. Shen, Z. Xu, and H. Wang, Int. J. Mod. Phys. B **19**, 275 (2005).
[48] D. J. Rahn, S. Hellmann, M. Kalläne, C. Sohrt, T. K. Kim, L. Kipp, and K. Rossnagel, Phys. Rev. B **85**, 224532 (2012).
[49] I. Guillamón, H. Suderow, S. Vieira, L. Cario, P. Diener, and P. Rodière, Phys. Rev. Lett. **101**, 166407 (2008).